

Regularized inversion of diatomic vibration-rotation spectral data: A functional sensitivity analysis approach

Hoon Heo, Tak-San Ho, Kevin K. Lehmann, and Herschel Rabitz
Department of Chemistry, Princeton University, Princeton, New Jersey 08544

(Received 20 February 1992; accepted 1 April 1992)

We present a stable and accurate inversion method for extracting potentials from spectroscopic data of diatomic molecules. The method, which was developed previously for inverting scattering data, is based on first-order functional sensitivity analysis in conjunction with the Tikhonov regularization, singular system analysis, and an exact transformation technique. Besides being numerically stable, it requires neither explicit functional forms nor special basis function expansions for the potential corrections when solving the corresponding linearized integral equation. Instead, we solve the linear equation directly in terms of the probability densities of the unperturbed vibrotation eigenstates. For illustration, we consider the ground electronic state of the H_2 molecule. Inversions have been carried out for simulated data free of noise and for those with noise of magnitude comparable to realistic experimental errors. It is found that in both cases, a relatively large deviation of the starting reference potential from the truth may be tolerated to still accurately recover the intended one. The propagation of the spectral errors is analyzed in detail based on the linearization assumption. The variance of the recovered potential reveals the reliability of various regions of the recovered potential.

I. INTRODUCTION

The determination of the interatomic/molecular and intramolecular potentials from experimental measurements is fundamental for understanding many important molecular properties. While the former has been studied using mainly scattering data, the latter has been scrutinized intensively using spectroscopic data. These two undertakings complement each other, thus, along with *ab initio* calculations, they can provide a comprehensive picture of the system under study. Very recently, we have developed a stable, efficient, and accurate inversion method,¹ the regularized inverse functional sensitivity analysis (hereafter RIFSA) method, within the framework of the functional sensitivity analysis, the Tikhonov regularization, and the singular system analysis for a finite amount of data. The method has been applied successfully to extracting weakly bound state potentials of inert gas pairs^{1(a),1(b)} and gas-surface potentials^{1(c)} from corresponding simulated scattering data. The present paper is intended as an initial extension of the method to inverse spectroscopic problems by explicitly considering diatomic vibrotation spectral measurements as input data to recover the underlying intramolecular potential. The ultimate goal is the treatment of polyatomic spectral inversion.

For many years, the Rydberg-Klein-Rees (RKR) method² has been the main vehicle for extracting potential energy curves of diatomic molecules from the measured vibrotation spectral data. It is, however, a first-order semiclassical approximation and generally applicable only to very restricted cases, e.g., potentials with a single minimum. Although its precision can be further increased by including higher-order corrections,³ its extension to more complicated systems has been particularly difficult.⁴ The inverse perturbation analysis (IPA) method of Kosman

and Hinze⁵ is a full quantum mechanical variational method originally intended to improve upon the RKR potentials and has been applied to various systems including polyatomic molecules.⁶ One key feature of the IPA method is the use of a basis set expansion for the potential corrections. This not only raises a serious issue of how to properly decide on a particular set of basis functions, but suffers from likely stability problems when the number of basis functions becomes large. Although over years many modifications on the IPA method have been made,^{7,8} thus widening the scope of its applications, these endeavors have only focused on the choice of the basis functions and have not adequately addressed the two aforementioned issues, particularly the stability problem caused by a finite amount of data and possibly also by the data errors.

The RIFSA method applied to inverse spectroscopic problems is based on the same first-order perturbation theory as the IPA method. The former, however, does not make use of a finite basis function expansion when solving the corresponding linear integral equation relating small changes in the bound state energies and the underlying potential. Rather, the linearized equation or its transformed equivalence is solved within the framework of the Tikhonov regularization method for linear ill-posed problems.⁹ Specifically, the approximate solution of the linear equation is obtained by minimizing a quadratic functional of the desired potential correction, subject explicitly to any *a priori* constraints on the potential. By invoking singular system analysis,¹⁰ we can readily form a set of orthonormal basis functions directly from the probability densities of the unperturbed counterparts of the bound states considered. In terms of these functions, we can evaluate easily the potential correction and can gain further insights, e.g., the spatial resolution and the information content of the data. Furthermore, the Tikhonov regularization procedure al-

lows us to effectively treat realistic spectral data contaminated with measurement errors. We will explicitly address noisy vibrotation energy spectra in the present simulated inverse diatomic spectroscopic problems. Finally, we perform a detailed statistical analysis on the errors of the recovered potential due to the spectral errors by computing a covariance matrix based on the linearization assumption.

In Sec. II, we describe the algorithm of inverse spectroscopic problems within the framework of diatomic vibrotation energy spectra. Explicitly, the Tikhonov regularization procedure and the singular system analysis are introduced in conjunction with exact transformations from the original linear integral equation to its various equivalent forms. This is followed by Sec. III, where a discussion is presented on the propagation of spectral data errors into the recovered potential. Then in Sec. IV, we analyze the results obtained from a case study on the ground electronic potential of the hydrogen molecule. Both noise-free and noisy simulated spectral data are used in our calculations. Finally, in Sec. V, we give a brief summary.

II. REGULARIZED INVERSION PROCEDURE

For simplicity, we consider a $^1\Sigma$ state potential $V(R)$ of a diatomic molecule. The vibrotational energy eigenvalues E_{vj} and the corresponding eigenfunctions $\psi_{vj}(R)$ are prescribed by the following radial Schrödinger equation:

$$\left\{ -\frac{\hbar^2}{2\mu} \frac{d^2}{dR^2} + \left[V(R) + \frac{\hbar^2}{2\mu R^2} j(j+1) \right] \right\} \psi_{vj}(R) = E_{vj} \psi_{vj}(R) \quad (1)$$

subject to the boundary conditions $\psi_{vj}(0) = 0$ and $\psi_{vj}(\infty) = 0$. Here μ is the reduced mass, and v and j are vibrational and rotational quantum numbers, respectively. We note that for electronic states other than $^1\Sigma$, the centrifugal potential term should be changed according to the particular angular momentum coupling case under study. Our purpose here is to recover the potential $V(R)$ as precisely as possible from the vibrotation spectral energies E_{vj}^{exp} which may be contaminated with random errors. With no loss of generality, we shall assume that the errors ϵ_{vj} 's are normally distributed and satisfy the following two relations:

$$\langle \epsilon_{vj} \rangle = 0 \quad (2)$$

and

$$\langle \epsilon_{vj} \epsilon_{v'j'} \rangle = \sigma_{vj}^2 \delta_{vv'} \delta_{jj'} \quad (3)$$

Here $\langle \dots \rangle$ denotes statistical expectation over an ensemble of measurements, σ_{vj}^2 is the variance which may be different for different levels, and δ_{pq} is the Kronecker delta. Now the experimental vibrotational eigenenergies are expressed as

$$E_{vj}^{\text{exp}} = E_{vj}^{\text{exact}} + \epsilon_{vj} \quad (4)$$

with E_{vj}^{exact} specifically standing for the exact, noise-free eigenenergies for the true potential $V(R)$.

In general, the functional relation between the eigenenergies and the underlying potential $V(R)$ is nonlinear.

While solving the forward problem based on Eq. (1), i.e., computing the bound state energies E_{vj} when the potential $V(R)$ is given, is quite straightforward, the inverse procedure, i.e., obtaining the potential $V(R)$ from a given set of bound energies, can be very difficult either analytically or numerically. In practice, the inverse problem may be solved iteratively by invoking first-order perturbation theory which yields the linear relation

$$\delta E_{vj} = \int_0^\infty \frac{\delta E_{vj}}{\delta V(R)} \delta V(R) dR \quad (5)$$

with

$$\frac{\delta E_{vj}}{\delta V(R)} = |\psi_{vj}^0(R)|^2$$

between small changes $\delta E_{vj} = E_{vj} - E_{vj}^0$ in the eigenenergies and small perturbations $\delta V(R) = V(R) - V_0(R)$ in the potential. The eigenfunctions $\psi_{vj}^0(R)$ and eigenvalues E_{vj}^0 are the solutions to Eq. (1) for the reference potential $V_0(R)$. Through the iterations, we update the potential by adding to it the potential correction $\delta V(R)$ which is obtained by solving Eq. (5) or its equivalences (see below), i.e.,

$$V(R) = V_0(R) + \delta V(R), \quad (6)$$

until a convergence criterion is fulfilled.

The linear integral equation (5) is usually ill conditioned, especially when taking into account the biases caused by the underlying nonlinearity and the data errors. Thus it must be solved with care along with any *a priori* constraints on the potential correction $\delta V(R)$. In many situations, a constraint involving high-order derivatives of $\delta V(R)$ is needed to render the recovered potential smooth and physically meaningful. To facilitate the numerical computations, we first define the quantity

$$\delta E_{vj} \equiv E_{vj}^{\text{exp}} - E_{vj}^0 \quad (7)$$

with the data errors contained explicitly in the quantity E_{vj}^{exp} . We then rewrite Eq. (5) as follows:

$$\delta E_{vj} = \int_0^\infty K_{vj}(R) \delta V(R) w(R) dR, \quad (8)$$

where

$$w(R) K_{vj}(R) = \frac{\delta E_{vj}}{\delta V(R)}.$$

It is easily seen that if the weighting factor $w(R)$ assumes the form R^2 , the kernel $K_{vj}(R)$ is simply the probability density $|\psi_{vj}^0(R)|^2/R^2$ for the vibrotational bound state of the starting potential $V_0(R)$ at each iteration. We note that it may be beneficial to weight the data E_{vj}^{exp} and E_{vj}^0 in Eq. (7), and thus Eq. (8), according to the variance σ_{vj}^2 . Finally, Eq. (8) can be further transformed, via integration by parts, into an equivalent form as follows^{1(b)}:

$$\delta E_{vj} = \int_0^\infty K_{vj}^{[n]}(R) [R^n \times \delta V^{(n)}(R)] w(R) dR \quad (9)$$

under the assumption

$$[-R^k w(R) K_{vj}^{[k]}(R) \times \delta V^{(k-1)}(R)]|_0^\infty = 0, \quad k=1,2,\dots,n. \quad (10)$$

Here the kernels $K_{vj}^{[k]}(R)$ satisfy the recurrence relation

$$R^k w(R) K_{vj}^{[k]}(R) = - \int_0^R K_{vj}^{[k-1]}(R') R'^{k-1} w(R') dR' \quad (11)$$

with

$$K_{vj}^{[0]}(R) \equiv K_{vj}(R)$$

and the quantity $\delta V^{(n)}(R)$ is simply the n th-order derivative of $\delta V(R)$ with respect to the interatomic distance R , namely,

$$\delta V^{(n)}(R) = \frac{d^n}{dR^n} \delta V(R). \quad (12)$$

The assumption in Eq. (10) is likely to hold because the probability density of each bound state falls off exponentially away from the corresponding classical turning points and most of the diatomic potentials approach zero quickly at large separation.^{1(b)} The formulation in Eq. (9) is equivalent to Eq. (8), but the former one now allows for the convenient introduction of a cost such that $\delta V^{(n)}$ is minimized while seeking the solution $\delta V(R)$.

Within the framework of the Tikhonov regularization procedure, Eq. (9) can be solved by minimizing the following quadratic functional²:

$$\Phi(\alpha, R^n \times \delta V^{(n)}) = \|K^{[n]}(R^n \times \delta V^{(n)}) - \delta E\|_{\mathbf{D}}^2 + \alpha \|R^n \times \delta V^{(n)}\|_{\mathfrak{R}}^2, \quad (13)$$

where

$$\begin{aligned} & \|K^{[n]}(R^n \times \delta V^{(n)}) - \delta E\|_{\mathbf{D}}^2 \\ & \equiv \sum_{vj} \left[\int_0^\infty K_{vj}^{[n]}(R) R^n \delta V^{(n)}(R) w(R) dR - \delta E_{vj} \right]^2, \end{aligned} \quad (14)$$

and

$$\|R^n \times \delta V^{(n)}\|_{\mathfrak{R}}^2 \equiv \int_0^\infty [R^n \delta V^{(n)}(R)]^2 w(R) dR. \quad (15)$$

Here \mathbf{D} and \mathfrak{R} represent the discrete eigenvalue space and the continuous distance space, respectively. The regularization parameter α is an arbitrary positive number yet to be chosen to balance the residual $\|K^{[n]}(R^n \times \delta V^{(n)}) - \delta E\|_{\mathbf{D}}^2$ and the smoothness constraint $\|R^n \times \delta V^{(n)}\|_{\mathfrak{R}}^2$. As proposed previously, the value of α can be optimally determined at each iteration by minimizing the following functional:

$$J(\alpha) \equiv \|E^{\text{expt}} - E^{\text{calc}}\|_{\mathbf{D}}^2, \quad (16)$$

which measures the difference between input eigenenergies E_{vj}^{expt} and the calculated ones E_{vj}^{calc} for an arbitrarily chosen α value. Typically we start with a large [usually much larger than the largest singular value of the kernel $K_{vj}^{[n]}(R)$] positive number of α . As α is gradually decreased,

the magnitude of the functional $J(\alpha)$ first decreases because more weight is placed on the residual in Eq. (13). When an appropriate α value, the optimal α , is located, $J(\alpha)$ arrives at a minimum. As the α value is further reduced, $J(\alpha)$ usually increases monotonically because more higher frequency components of the kernel $K_{vj}^{[n]}(R)$ are involved. Moreover, a higher-order constrained derivative usually inflicts heavier penalty on the solution, thus likely producing smoother results for $V(R)$; however, if extreme smoothness is sought, some essential structure in $V(R)$ may be lost. Consequently, it is necessary to properly choose a value of n for the functional defined in Eq. (13) to yield an adequate potential correction.

Assuming a total number of N input vibrotation energy levels, for given α and n , we can readily produce the solution which minimizes the functional in Eq. (13) in terms of the singular system¹⁰ of the kernel $K_{vj}^{[n]}(R)$ designated as $\{\omega_i^{[n]2}; u_i^{[n]}, v_i^{[n]}\}$, $i=1,2,\dots,N$.

$$\delta V_{\alpha}^{(n)}(R) = \frac{1}{R^n} \sum_{i=1}^N \frac{\omega_i^{[n]} (\delta E, u_i^{[n]})_{\mathbf{D}}}{\omega_i^{[n]2} + \alpha} v_i^{[n]}(R) \quad (17)$$

with the inner product defined as

$$(\delta E, u_i^{[n]})_{\mathbf{D}} \equiv \sum_{vj} \delta E_{vj} u_{i,vj}^{[n]}. \quad (18)$$

The singular vectors $\{u_i^{[n]}\}$ and the singular functions $\{v_i^{[n]}\}$ have the following orthonormal relations and satisfy the following shifted eigenvalue equations:

$$\begin{aligned} (u_k^{[n]}, u_l^{[n]})_{\mathbf{D}} &= \sum_{vj} u_{k,vj}^{[n]} u_{l,vj}^{[n]} = \delta_{kl} \\ \langle v_k^{[n]} | v_l^{[n]} \rangle_{\mathfrak{R}} &= \int_0^\infty v_k^{[n]}(R) v_l^{[n]}(R) w(R) dR = \delta_{kl} \end{aligned} \quad (19)$$

$$K^{[n]} v_i^{[n]} = \omega_i^{[n]} u_i^{[n]}, \quad K^{[n]\dagger} u_i^{[n]} = \omega_i^{[n]} v_i^{[n]}, \quad (20)$$

with $K^{[n]\dagger}$ denoting the adjoint of $K^{[n]}$. Furthermore, the singular values $\{\omega_i^{[n]2}\}$ are conveniently arranged in descending order, i.e., $\omega_1^{[n]2} \geq \omega_2^{[n]2} \geq \dots \geq \omega_{N-1}^{[n]2} \geq \omega_N^{[n]2} > 0$. Finally, the potential correction at each iteration can be obtained by using the following integral relation:

$$\delta V^{(k-1)}(R) = - \int_R^\infty \delta V^{(k)}(R') dR', \quad k=1,2,\dots,n \quad (21)$$

with the assumption that

$$\delta V^{(k)}(\infty) = 0, \quad \forall k=0,1,2,\dots,n-1 \quad (22)$$

which holds for realistic interatomic potentials.

To end this section, we describe briefly the criteria for stopping the iterative inversion procedure. Generally, the starting reference potential $V_0(R)$ may be quite far away from the intended one, thus the difference between their corresponding vibrotation eigenenergies may be large compared to the data errors. Thus the iterations proceed by choosing the regularization parameter α by minimization of Eq. (16). Gradually the recovered potential becomes closer to the intended one and yields eigenenergies which

better resemble the input data. When the calculated data are in good agreement with the input data, we can stop the iteration procedure. In practice, we have two distinct stopping criteria for noise-free and noisy cases. For the former case, we terminate the iteration as soon as the data difference, which is to be measured by the quantity $J(\alpha)$ of Eq. (16), falls below a prescribed small tolerance. While for the latter case, we stop the inversion procedure as soon as the following criterion is fulfilled, assuming normally distributed errors with variances σ_{vj}^2 :

$$\chi^2 = \sum_{vj} \frac{(E_{vj}^{\text{expt}} - E_{vj}^{\text{calc}})^2}{\sigma_{vj}^2} < N \quad (23)$$

with the amount of data N so that we may not overfit the data.

III. THE EFFECT OF DATA ERRORS IN THE INVERSION

In this section, we study the possible effect on the recovered potential $V(R)$ of the normally distributed random errors contained in the input vibrotation eigenenergies E_{vj}^{expt} . Since it is difficult to give a quantitative error analysis about the solution for any nonlinear inverse problem, we shall confine ourselves to the linearized equation (5). Although it is likely that bias will occur due to the nonlinear nature of the problem, our analysis based on the linearization assumption shall provide qualitatively useful information. Furthermore, for simplicity, we shall assume that the normally distributed errors are characterized by the same constant variance σ^2 .

The statistical uncertainty of the recovered potential depends not only on the variance of the errors, but also on the regularization procedure in general. Given the regularization parameter α and the order n of the derivative constraint, we can produce the following approximate linear inverse relation from Eqs. (17) and (21)

$$\delta V_\alpha(R) = \sum_{vj} \frac{\delta V_\alpha(R)}{\delta E_{vj}} \delta E_{vj} \quad (24)$$

where

$$\begin{aligned} \frac{\delta V_\alpha(R)}{\delta E_{vj}} &= (-1)^n \int_R^\infty \int_{R_1}^\infty \int_{R_2}^\infty \cdots \int_{R_{n-1}}^\infty dR_1 dR_2 \cdots \\ &\quad \times dR_n \frac{\delta V_\alpha^{(n)}(R_n)}{\delta E_{vj}} \end{aligned} \quad (25)$$

with

$$\frac{\delta V_\alpha^{(n)}(R)}{\delta E_{vj}} = \frac{1}{R^n} \sum_{i=1}^N \frac{\omega_i^{[n]} u_{i,vj}^{[n]}}{\omega_i^{[n]^2} + \alpha} v_i^{[n]}(R). \quad (26)$$

By invoking Eqs. (2) and (3), we can readily arrive at the following expression for the covariance matrix of the potential correction:

$$\langle \delta V_\alpha(R) \delta V_\alpha(R') \rangle = \sigma^2 \sum_{vj} \frac{\delta V_\alpha(R)}{\delta E_{vj}} \frac{\delta V_\alpha(R')}{\delta E_{vj}}. \quad (27)$$

If we further make use of the orthonormal relation in Eq. (19), the variance of the potential correction takes on the simple form

$$\langle \delta V_\alpha(R) \delta V_\alpha(R) \rangle = \sigma^2 \sum_{i=1}^N \left(\frac{\omega_i^{[n]}}{\omega_i^{[n]^2} + \alpha} \right)^2 W_i^{[n]}(R) \quad (28)$$

with

$$\begin{aligned} W_i^{[n]}(R) &\equiv \left[\int_R^\infty \int_{R_1}^\infty \int_{R_2}^\infty \cdots \int_{R_{n-1}}^\infty \right. \\ &\quad \left. \times dR_1 dR_2 \cdots dR_n \frac{v_i^{[n]}(R_n)}{R_n^n} \right]^2. \end{aligned} \quad (29)$$

Here we note that the variance $\langle \delta V_\alpha(R) \delta V_\alpha(R) \rangle$ is linearly proportional to the data error variance σ^2 . Moreover, its magnitude increases monotonically as α becomes smaller. As a result, the ratio of the potential error to the data error can become very large if we overfit the data by choosing too small an α value. On the other hand, the resolution of the potential may be very poor if we try to oversuppress the influence of the data error by choosing too large an α value. Finally, the variance of the potential should reveal the trustworthiness of various regions of the recovered potential in accordance with the information content of the input data as regulated by the R -dependent weighting factor $W_i^{[n]}(R)$. This will be addressed in detail in the next section when we analyze our results.

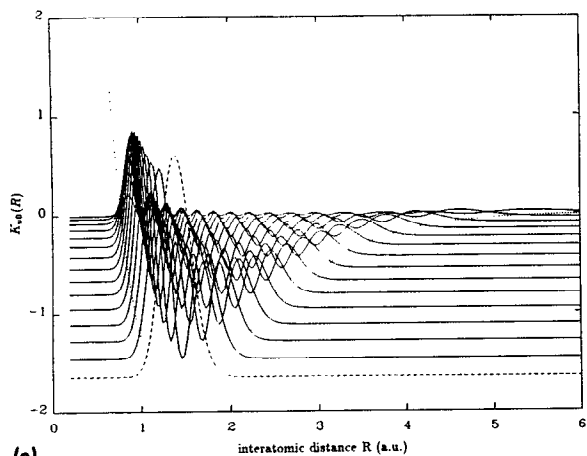
IV. RESULTS AND DISCUSSIONS: THE GROUND ELECTRONIC STATE OF THE HYDROGEN MOLECULE

We consider the ground electronic state $X^1\Sigma_g^+$ of the hydrogen molecule. The Kolos/LeRoy-Schwartz potential¹¹ will be adopted as the model potential to be used to simulate the experimental vibrational spectra. Here the radial Schrödinger equation (1) is solved using the Numerov algorithm to determine the bound states and the corresponding wave functions.¹² In most of our calculations, we shall consider all the bound vibrational states for the rotational quantum numbers $j=0,1,2,\dots,9$; the total number N of input levels in this "full" case is equal to 142. Although the ultimate goal is to recover potentials from true experimental data, the studies here are useful as a guide to how much data is really needed for the inversion and how data errors can affect the inversion outcome. In the rest of this section, we shall use atomic units unless otherwise stated.

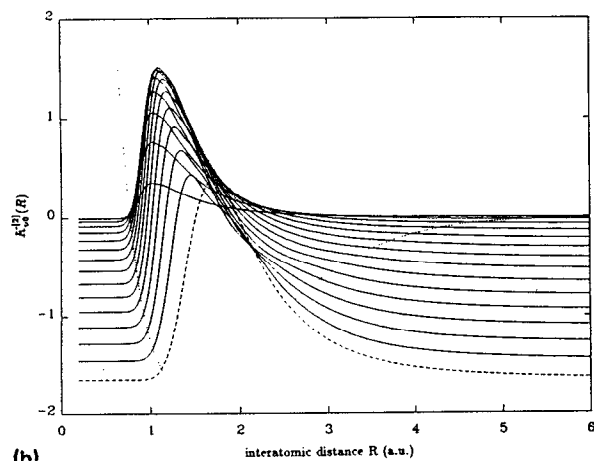
The recovered potential based on our inversion scheme is expected to be nearly independent of the starting reference potential as demonstrated previously.¹ We will assume that the starting reference potential in the inversion is a Morse potential¹³

$$V_0(R) = D_e(e^{-2a(R-R_e)} - 2e^{-a(R-R_e)}) \quad (30)$$

characterized by a dissociation energy D_e , a minimum position R_e , and a length scaling parameter a . In the numerical implementation, we need to choose the weighting factor $w(R)$ and the order n of the derivative constraint in



(a)



(b)

FIG. 1. Functional sensitivity densities as functions of the interatomic distance R and the vibrational quantum number ν (unlabeled) for $j=0$. (a) Kernel $K_{\nu j}^{[0]}(R)$ and (b) Kernel $K_{\nu j}^{[2]}(R)$. The calculations were done for the Kolos/Le Roy-Schwartz potential (dotted curve, multiplied by 10) for the ground electronic state $X^1\Sigma_g^+$ of the H_2 molecule. The vibrational quantum numbers are $\nu=0,1,2,\dots,14$. $K_{00}^{[0]}(R)$ and $K_{00}^{[2]}(R)$ are shown as dashed curves, and the rest as solid curves. For plotting purposes, the eigenenergies E_{ν}^{expt} (after being multiplied by 10) have been added to the quantities $K_{\nu 0}^{[0]}(R)$ and $K_{\nu 0}^{[2]}(R)$.

Eq. (9). In this work, we have chosen $w(R) = R^2$ and assumed $n=2$. The choice $n=2$ yielded very satisfactory results for cases considered below, although we have also found equally good results with $n=3$ or 4. The real significance of using a higher-order constraint can be seen clearly from Figs. 1(a) and 1(b) in which the kernels $K_{\nu j}^{[0]}(R)$ and $K_{\nu j}^{[2]}(R)$ are displayed as functions of the vibrational quantum number ν for $j=0$ and the interatomic distance R . It is found that the kernel for $n=2$ becomes smoother than the case $n=0$, while still resembling closely the global character of the latter kernel. The net result is thus to roll out the higher frequency components of the original kernel, very much like a preconditioning process in the conjugate gradient procedure for solving linear algebraic problems,¹⁴ with the intention of yielding more stability. In the following, we present our first inversion results for (i) noise-free data, and then for (ii) normally distributed noisy data. Finally, we discuss in depth the

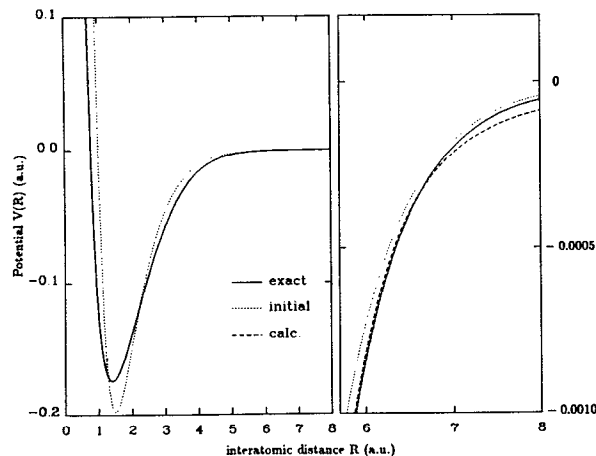


FIG. 2. Interatomic potentials of $X^1\Sigma_g^+$ of H_2 —the Kolos/Le Roy-Schwartz potential (assumed exact in the work) (solid line); Morse type potential with $D_e = 0.198$, $R_e = 1.5$, and $a = 1.4$ (numbers are in atomic units) (dotted line); recovered potential at iteration 25 (dashed line). The input consisted of 142 noise-free eigenenergies, i.e., all vibrational levels for $j=0,1,2,\dots,9$ were used for the inversion.

effect of the data errors on the recovered potential based on the linear assumption of Eq. (8).

A. Noise free data

In Fig. 2, we present the results, using the full data set with 142 bound states defined above, for the recovered potential along with the model potential and the initial one which is a Morse form with $D_e = 0.198$, $R_e = 1.5$, and $a = 1.4$ in Eq. (30). It is found that the recovered potential closely resembles the model potential over the whole region, but is slightly lower than the dissociation threshold of its model counterpart. The discrepancies observed at the very small distances and at the large distances, here $R > 7$, can be attributed to the lack of information content in the input data about these two regions. Further improvement in these regions may be possible if more rotational quantum numbers or quasibound (resonant) states are included in the input, or if scattering data are involved. Moreover, we compare the vibrotation eigenenergies for the recovered potential with the input data, see Table I. The agreement between the two sets of the data is generally up to the seventh decimal point for every level except for a few of the highest vibrational levels. We comment that we have also performed the calculations with other starting reference potentials assuming various well depths and minimum positions and found results quite comparable to those above for relatively large initial deviations from the true potential.

For a clear understanding of the dependence of the recovered potential on the amount of the input data used in the inversion, we show in Fig. 3 results for 80 input levels, i.e., eight vibrational levels each with the first ten rotational states. As expected the potential is only well recovered over a range approximately spanned up to the highest classical turning points.

TABLE I. Comparison of the energy eigenvalues (noise-free case). Recovered eigenvalues are the result of 25 iterations with the same starting potential as in Fig. 2. All numbers are in atomic units.

$\nu \setminus j$	0	1	2	3	4	5	6	7	8	9
0	-0.164 563 9 ^a	-0.164 024 0	-0.162 949 1	-0.161 349 1	-0.159 238 1	-0.156 634 5	-0.153 560 1	-0.150 039 8	-0.146 100 8	-0.141 771 9
	-0.164 563 9 ^b	-0.164 024 0	-0.162 949 1	-0.161 349 1	-0.159 238 1	-0.156 634 5	-0.153 560 1	-0.150 039 8	-0.146 100 8	-0.141 771 9
1	-0.145 600 4	-0.145 087 4	-0.144 066 3	-0.142 546 5	-0.140 541 6	-0.138 069 5	-0.135 151 2	-0.131 810 6	-0.128 073 9	-0.123 969 1
	-0.145 600 4	-0.145 087 4	-0.144 066 3	-0.142 546 5	-0.140 541 6	-0.138 069 5	-0.135 151 2	-0.131 810 6	-0.128 073 9	-0.123 969 1
2	-0.127 709 5	-0.127 222 9	-0.126 254 4	-0.124 812 9	-0.122 912 0	-0.120 568 5	-0.117 803 0	-0.114 638 6	-0.111 100 4	-0.107 215 4
	-0.127 709 5	-0.127 222 9	-0.126 254 4	-0.124 812 9	-0.122 912 0	-0.120 568 5	-0.117 803 0	-0.114 638 6	-0.111 100 4	-0.107 215 4
3	-0.110 869 0	-0.110 408 3	-0.109 491 5	-0.108 127 4	-0.106 328 8	-0.104 112 2	-0.101 497 5	-9.850 691(-2)	-9.516 492(-2)	-9.149 758(-2)
	-0.110 869 0	-0.110 408 3	-0.109 491 5	-0.108 127 4	-0.106 328 8	-0.104 112 2	-0.101 497 5	-9.850 691(-2)	-9.516 492(-2)	-9.149 758(-2)
4	-9.506 493(-2)	-9.463 005(-2)	-9.376 461(-2)	-9.247 720(-2)	-9.078 030(-2)	-8.868 992(-2)	-8.622 521(-2)	-8.340 783(-2)	-8.026 151(-2)	-7.681 149(-2)
	-9.506 495(-2)	-9.463 006(-2)	-9.376 463(-2)	-9.247 721(-2)	-9.078 030(-2)	-8.868 994(-2)	-8.622 522(-2)	-8.340 783(-2)	-8.026 151(-2)	-7.681 149(-2)
5	-8.029 281(-2)	-7.988 372(-2)	-7.906 979(-2)	-7.785 931(-2)	-7.626 444(-2)	-7.430 076(-2)	-7.198 684(-2)	-6.934 379(-2)	-6.639 471(-2)	-6.316 421(-2)
	-8.029 281(-2)	-7.988 373(-2)	-7.906 980(-2)	-7.785 933(-2)	-7.626 446(-2)	-7.430 077(-2)	-7.198 685(-2)	-6.934 381(-2)	-6.639 472(-2)	-6.316 421(-2)
6	-6.655 857(-2)	-6.617 563(-2)	-6.541 388(-2)	-6.428 141(-2)	-6.279 007(-2)	-6.095 506(-2)	-5.879 454(-2)	-5.632 912(-2)	-5.358 142(-2)	-5.057 560(-2)
	-6.655 855(-2)	-6.617 562(-2)	-6.541 388(-2)	-6.428 143(-2)	-6.279 010(-2)	-6.095 509(-2)	-5.879 456(-2)	-5.632 913(-2)	-5.358 143(-2)	-5.057 560(-2)
7	-5.388 050(-2)	-5.352 439(-2)	-5.281 619(-2)	-5.176 386(-2)	-5.037 899(-2)	-4.867 650(-2)	-4.667 421(-2)	-4.439 244(-2)	-4.185 350(-2)	-3.908 134(-2)
	-5.388 042(-2)	-5.352 433(-2)	-5.281 617(-2)	-5.176 387(-2)	-5.037 902(-2)	-4.867 652(-2)	-4.667 424(-2)	-4.439 246(-2)	-4.185 352(-2)	-3.908 135(-2)
8	-4.229 167(-2)	-4.196 350(-2)	-4.131 114(-2)	-4.034 242(-2)	-3.906 878(-2)	-3.750 499(-2)	-3.566 872(-2)	-3.358 016(-2)	-3.126 163(-2)	-2.873 718(-2)
	4.229 149(-2)	-4.196 337(-2)	-4.131 108(-2)	-4.034 241(-2)	-3.906 880(-2)	-3.750 500(-2)	-3.566 872(-2)	-3.358 017(-2)	-3.126 165(-2)	-2.873 720(-2)
9	-3.184 355(-2)	-3.154 502(-2)	-3.095 192(-2)	-3.007 205(-2)	-2.891 684(-2)	-2.750 107(-2)	-2.584 250(-2)	-2.396 153(-2)	-2.188 090(-2)	-1.962 532(-2)
	-3.184 328(-2)	-3.154 484(-2)	-3.095 185(-2)	-3.007 207(-2)	-2.891 687(-2)	-2.750 106(-2)	-2.584 246(-2)	-2.396 150(-2)	-2.188 089(-2)	-1.962 534(-2)
10	-2.261 092(-2)	-2.234 450(-2)	-2.181 567(-2)	-2.103 233(-2)	-2.000 608(-2)	-1.875 199(-2)	-1.728 831(-2)	-1.563 619(-2)	-1.381 948(-2)	-1.186 457(-2)
	-2.261 062(-2)	-2.234 433(-2)	-2.181 568(-2)	-2.103 244(-2)	-2.000 617(-2)	-1.875 197(-2)	-1.728 821(-2)	-1.563 609(-2)	-1.381 943(-2)	-1.186 455(-2)
11	-1.469 907(-2)	-1.446 835(-2)	-1.401 104(-2)	-1.333 536(-2)	-1.245 342(-2)	-1.138 107(-2)	-1.013 775(-2)	-8.746 332(-3)	-7.233 178(-3)	-5.628 423(-3)
	-1.469 878(-2)	-1.446 824(-2)	-1.401 117(-2)	-1.333 561(-2)	-1.245 358(-2)	-1.138 104(-2)	-1.013 758(-2)	-8.746 167(-3)	-7.233 097(-3)	-5.628 359(-3)
12	-8.254 141(-3)	-8.064 360(-3)	-7.689 265(-3)	-7.137 741(-3)	-6.423 056(-3)	-5.562 832(-3)	-4.579 147(-3)	-3.498 889(-3)	-2.354 643(-3)	-1.186 807(-3)
	-8.253 968(-3)	-8.064 390(-3)	-7.689 532(-3)	-7.138 073(-3)	-6.423 201(-3)	-5.562 690(-3)	-4.578 880(-3)	-3.498 741(-3)	-2.354 615(-3)	-1.186 693(-3)
13	-3.478 573(-3)	-3.337 780(-3)	-3.061 384(-3)	-2.659 858(-3)	-2.149 187(-3)	-1.551 459(-3)	-8.962 451(-4)	-2.244 025(-4)		
	-3.478 668(-3)	-3.338 006(-3)	-3.061 701(-3)	-2.660 037(-3)	-2.149 032(-3)	-1.551 118(-3)	-8.961 866(-4)	-2.246 772(-4)		
14	-6.522 291(-4)	-5.743 278(-4)	-4.259 821(-4)	-2.232 728(-4)						
	-6.523 897(-4)	-5.743 313(-4)	-4.257 177(-4)	-2.234 122(-4)						

^aInput noise-free data.

^bRecovered data.

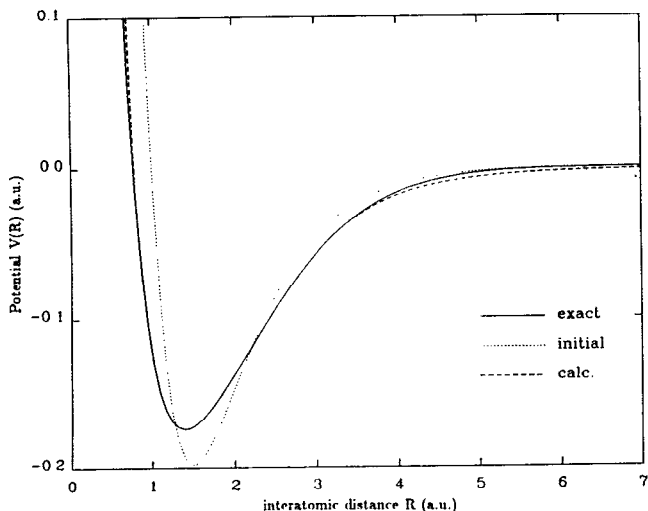


FIG. 3. Recovered potential from an insufficient data set. Only the lowest eight vibrational levels for $j=0,1,2,\dots,9$ were used. See the caption of Fig. 2 for more details.

B. Normally distributed noisy data

Here the input vibration eigenenergies contain computer simulated errors which are normally distributed. It is further assumed that the errors are characterized by the same variance σ^2 . Explicitly, we first produce a set of normally distributed random numbers with a vanishing mean and a standard deviation equal to 0.1% of the dissociation energy of the Kolos/Le Roy–Schwartz potential for hydrogen molecule, i.e., approximately 36 cm^{-1} . This is actually a rather large error and its constant variance is very significant for the higher energy levels. Then these random numbers are added to the numerically exact vibration eigenenergies corresponding to the Kolos/Le Roy–Schwartz potential. Finally, these error contaminated data are considered as the experimental input data E_{vj}^{expt} in Eq. (7) for the inversion.

It is found in Fig. 4 that the potential recovered using the full $N=142$, but noisy data set is in good agreement with the model potential. We, however, observed small fluctuations about the model potential. The relatively larger fluctuations at the small and large interatomic separations is likely caused by the relatively large noise in the levels close to the dissociation threshold; with the assumption of equal variance for every level, we expect a large noise-to-signal ratio for the higher energy levels. The good agreement of the repulsive parts of the recovered and the model potentials is likely only an artifact of the potential fluctuations. Finally, we observed that the eigenenergies of the recovered potential bear a close resemblance to the noiseless ones of the original model, rather than their noisy input counterpart (see Tables I and II). This may be understood as a result of our not overfitting the noisy data when the iteration is stopped according to the criterion Eq. (23); fitting the noisy data too well can often result in unwanted severe fluctuations in the recovered potential.

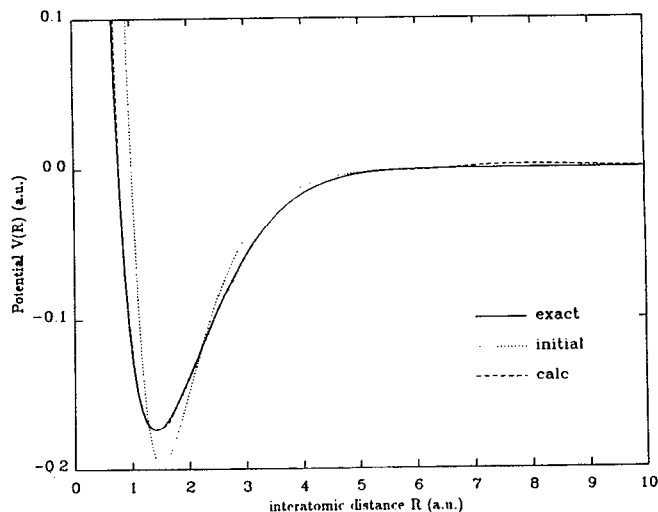


FIG. 4. Recovered potential from noisy eigenvalues. The allowed noise level in the eigenvalues was approximately 0.1% ($\sim 36\text{ cm}^{-1}$) of the dissociation energy of the ground electronic state $X^1\Sigma_g^+$ of H_2 . The data errors were assumed to be normally distributed with the same variance σ^2 . A total of 142 eigenvalues were used and the convergence criterion was met after eight iterations. See the caption of Fig. 2 for more details.

C. The effect of the data errors

The statistical uncertainty of the recovered potential due to the data errors can be quantified through the evaluation of the covariance matrix $\langle \delta V_\alpha(R) \delta V_\alpha(R') \rangle$.¹⁵ Here for simplicity, we again assumed that the normally distributed errors in the vibration energies are of the same variance. Therefore, the variance of the potential can be calculated using Eq. (28). Assuming the model potential as nominal, we display in Fig. 5 the variance ratio $\langle \delta V_\alpha(R) \delta V_\alpha(R) \rangle^{1/2} / \sigma$ as a function of the regularization parameter α and the interatomic distance R . We found, as expected from Eq. (28), that the variance ratio becomes larger, corresponding to greater uncertainty in the recovered potential, as the regularization parameter α becomes smaller. This is in agreement with the effective rank analysis for ill-posed problems of Gilliam *et al.*¹⁶ Moreover, the ratio is small in the potential well region and larger in the repulsive and longer range regions, reflecting the localized nature of the sensitivity density relating the bound state data and the underlying potential [see Fig. 1(a)].

Examining Fig. 5 more closely, we notice that as the parameter α becomes smaller and more high-frequency components of the corresponding kernel $K_{ij}(R)$ are retained, the variance ratio, as a function of the interatomic distance R , contains smaller scale structure. Thus, the resulting potential becomes better resolved spatially, but less accurate. Since the error ratio can be greater than unity in the well region when the regularization parameter is very small, we may need to choose carefully the parameter α at each inversion iteration so that the data errors do not cause a stability problem. In our calculations involving the normally distributed noisy data, the value of α lies between 10^{-4} and 10^{-8} throughout the iterations that lead to the results given in Fig. 4.

TABLE II. Comparison of the energy eigenvalues (noisy case). Simulated experimental values are obtained by adding errors (normally distributed with a standard deviation equal to 36 cm^{-1}) to the exact ones in the Table I. The convergence criterion in Eq. (23) was met at the eighth iteration. All numbers are in atomic units.

v, j	0	1	2	3	4	5	6	7	8	9
0	-0.164 351 1 ^a	-0.163 886 3	-0.162 897 7	-0.161 226 9	-0.158 933 1	-0.156 959 7	-0.153 315 1	-0.149 892 7	-0.146 338 3	-0.141 950 1
	-0.164 514 7 ^b	-0.163 982 9	-0.162 924 3	-0.161 348 3	-0.159 269 0	-0.156 704 0	-0.153 674 5	-0.150 204 3	-0.146 319 1	-0.142 046 1
1	-0.145 560 1	-0.145 065 7	-0.143 938 9	-0.142 643 2	-0.140 494 9	-0.137 908 2	-0.134 767 7	-0.131 736 4	-0.128 115 5	-0.123 896 5
	-0.145 641 1	-0.145 126 3	-0.144 101 6	-0.142 576 5	-0.140 565 1	-0.138 085 5	-0.135 159 9	-0.131 813 7	-0.128 075 2	-0.123 974 6
2	-0.127 683 9	-0.127 206 6	-0.126 255 9	-0.124 759 2	-0.122 988 2	-0.120 816 4	-0.117 641 6	-0.114 717 7	-0.111 249 1	-0.107 392 8
	-0.127 786 0	-0.127 303 5	-0.126 343 1	-0.124 913 6	-0.123 027 9	-0.120 702 4	-0.117 956 6	-0.114 812 5	-0.111 293 7	-0.107 425 4
3	-0.110 924 1	-0.110 603 2	-0.109 545 1	-0.108 083 6	-0.106 525 6	-0.104 373 1	-0.101 497 1	-9.854 822(-2)	-9.513 597(-2)	-9.180 684(-2)
	-0.111 021 0	-0.110 562 1	-0.109 648 4	-0.108 287 7	-0.106 491 8	-0.104 276 0	-0.101 658 9	-9.866 247(-2)	-9.531 131(-2)	-9.163 254(-2)
4	-9.486 107(-2)	-9.445 356(-2)	-9.376 007(-2)	-9.235 357(-2)	-9.073 965(-2)	-8.912 357(-2)	-8.614 728(-2)	-8.365 174(-2)	-8.039 319(-2)	-7.657 005(-2)
	-9.506 363(-2)	-9.463 272(-2)	-9.377 501(-2)	-9.249 854(-2)	-9.081 487(-2)	-8.873 866(-2)	-8.628 738(-2)	-8.348 105(-2)	-8.034 239(-2)	-7.689 697(-2)
5	-7.999 500(-2)	-7.971 703(-2)	-7.884 571(-2)	-7.780 701(-2)	-7.633 824(-2)	-7.429 313(-2)	-7.219 011(-2)	-6.929 565(-2)	-6.644 189(-2)	-6.326 403(-2)
	-8.017 665(-2)	-7.977 337(-2)	-7.897 159(-2)	-7.778 056(-2)	-7.621 330(-2)	-7.428 561(-2)	-7.201 490(-2)	-6.941 898(-2)	-6.651 536(-2)	-6.332 137(-2)
6	-6.643 067(-2)	-6.611 521(-2)	-6.548 863(-2)	-6.430 443(-2)	-6.276 327(-2)	-6.087 089(-2)	-5.904 840(-2)	-5.610 373(-2)	-5.353 149(-2)	-5.044 609(-2)
	-6.651 110(-2)	-6.612 655(-2)	-6.536 194(-2)	-6.422 629(-2)	-6.273 301(-2)	-6.089 969(-2)	-5.874 753(-2)	-5.630 022(-2)	-5.358 221(-2)	-5.061 664(-2)
7	-5.377 953(-2)	-5.364 995(-2)	-5.289 745(-2)	-5.170 918(-2)	-5.077 893(-2)	-4.854 548(-2)	-4.660 241(-2)	-4.421 238(-2)	-4.188 554(-2)	-3.927 185(-2)
	-5.386 737(-2)	-5.351 096(-2)	-5.280 206(-2)	-5.174 835(-2)	-5.036 112(-2)	-4.865 506(-2)	-4.664 829(-2)	-4.436 251(-2)	-4.182 323(-2)	-3.905 925(-2)
8	-4.222 456(-2)	-4.176 268(-2)	-4.130 502(-2)	-4.015 866(-2)	-3.923 580(-2)	-3.756 012(-2)	-3.572 833(-2)	-3.343 035(-2)	-3.124 772(-2)	-2.874 876(-2)
	-4.224 651(-2)	-4.191 830(-2)	-4.126 635(-2)	-4.029 946(-2)	-3.903 019(-2)	-3.747 402(-2)	-3.564 813(-2)	-3.357 031(-2)	-3.125 877(-2)	-2.873 359(-2)
9	-3.208 923(-2)	-3.164 576(-2)	-3.096 416(-2)	-3.017 928(-2)	-2.858 602(-2)	-2.732 767(-2)	-2.563 928(-2)	-2.399 319(-2)	-2.186 590(-2)	-1.960 503(-2)
	-3.182 262(-2)	-3.151 883(-2)	-3.091 528(-2)	-3.002 032(-2)	-2.884 707(-2)	-2.741 374(-2)	-2.574 335(-2)	-2.386 229(-2)	-2.179 761(-2)	-1.957 363(-2)
10	-2.275 829(-2)	-2.235 154(-2)	-2.169 690(-2)	-2.095 674(-2)	-2.008 890(-2)	-1.891 711(-2)	-1.717 147(-2)	-1.563 176(-2)	-1.394 642(-2)	-1.184 608(-2)
	-2.261 422(-2)	-2.234 874(-2)	-2.182 123(-2)	-2.103 859(-2)	-2.001 116(-2)	-1.875 278(-2)	-1.728 087(-2)	-1.561 673(-2)	-1.378 583(-2)	-1.181 787(-2)
11	-1.482 236(-2)	-1.434 147(-2)	-1.401 079(-2)	-1.318 725(-2)	-1.244 338(-2)	-1.149 053(-2)	-9.832 459(-3)	-8.629 030(-3)	-7.364 193(-3)	-5.615 145(-3)
	-1.469 775(-2)	-1.446 473(-2)	-1.400 237(-2)	-1.331 829(-2)	-1.242 445(-2)	-1.133 757(-2)	-1.007 937(-2)	-8.676 211(-3)	-7.158 508(-3)	-5.559 538(-3)
12	-8.019 847(-3)	-8.092 472(-3)	-7.615 283(-3)	-7.233 612(-3)	-6.431 421(-3)	-5.400 398(-3)	-4.572 474(-3)	-3.581 477(-3)	-2.317 330(-3)	-1.024 014(-3)
	-8.224 104(-3)	-8.035 562(-3)	-7.662 527(-3)	-7.113 236(-3)	-6.400 290(-3)	-5.540 590(-3)	-4.554 708(-3)	-3.465 754(-3)	-2.299 377(-3)	-1.090 277(-3)
13	-3.485 549(-3)	-3.396 344(-3)	-2.930 555(-3)	-2.346 196(-3)	-1.869 229(-3)	-1.333 389(-3)	-9.783 488(-4)	-7.140 534(-4)	...	
	-3.431 174(-3)	-3.285 601(-3)	-2.998 316(-3)	-2.577 907(-3)	-2.040 043(-3)	-1.412 629(-3)	-7.441 643(-4)	...		
14	-6.168 123(-4)	-5.873 393(-4)	-2.041 553(-4)	6.533 425(-5)						
	-6.267 890(-4)	-5.580 023(-4)	-4.239 453(-4)	-2.294 351(-4)						

^aInput noisy data.

^bRecovered data.

^cThis level was not bound in the recovered potential.

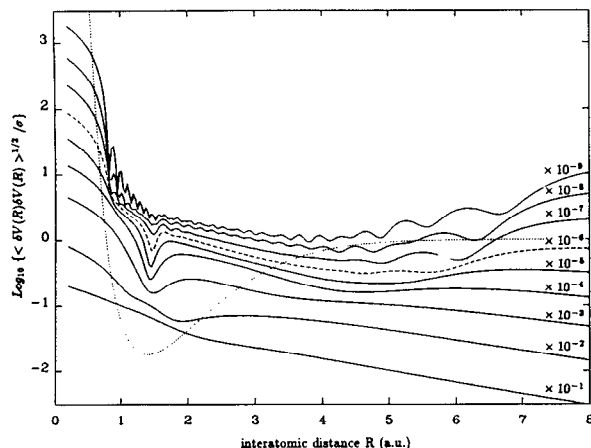


FIG. 5. The ratio of the potential variance to the input data variance $\langle \delta V_\alpha(R) \delta V_\alpha(R) \rangle^{1/2} / \sigma$ as a function of the interatomic distance R for different α values. At all distances, the ratio increases monotonically as α becomes smaller. The α values chosen here are obtained by multiplying the largest singular value $\omega^{[2]^2} = 2.1630$ of the kernel $K_\alpha^{[2]}(R)$ by the factors $10^{-1}, 10^{-2}, \dots, 10^{-9}$. Calculations were carried out assuming the Kolos/Le Roy-Schwartz potential of the H_2 molecule as the nominal potential, which is shown as a dotted curve for comparison with the behavior of the variance ratio.

In general, the error ratio rises much more quickly toward the steep inner potential wall than toward the soft outer wall. This, in large part, is due to a quicker drop of the probability densities toward the inner classical turning points than toward the outer classical turning points as indicated in Fig. 1(a) and, in small part, may be due to the conditions Eq. (22) imposed on the potential and its derivatives at the rightmost internuclear distance (~ 22 a.u.) in our numerical integration of the radial Schrödinger equation (1). All curves in Fig. 5 become zero at the rightmost distance (not shown) as a result of Eq. (22). It is interesting to see that the error ratio curve may contain a pronounced narrow minimum slightly to the right-hand side of the potential well minimum at a suitable value of α , e.g., $\alpha = 2.1630 \times 10^{-6}$ (the dashed curve). This minimum may be attributed to the $v=0$ bound states associated with various rotational quantum numbers j as seen clearly in Fig. 1(a) in which the probability density for $v=0$ and $j=0$ (the dashed curve) stands out among others and peaks at a distance to the immediate right-hand side of the potential minimum; the probability densities of $v=0$ states for nonzero j 's almost peak at the same distance because the well minimum positions of their corresponding effective radial potentials are close to each other. When α becomes very small, the error curve contains high-frequency oscillations from which the abovementioned narrow minimum becomes indistinguishable (see the top two curves in Fig. 5). Although the above error analysis is performed on the hydrogen molecule, similar observations may also be drawn about other diatomic molecules.

V. SUMMARY

We have shown that the RIFSA method can be used to accurately extract strongly bound interatomic potentials

from spectroscopic data. The electronic potential curve of $H_2 X^1\Sigma_g^+$ state recovered from simulated bound state data by this method was almost converged to the assumed "exact" potential over all the interatomic distances. Small discrepancies observed at very small and large separations are attributed to the lack of corresponding relevant information in the input data and the results may be further improved by including more rotational states or even scattering data. We also presented a result for when the input eigenenergies are contaminated with measurement errors by considering the computer-simulated normally distributed errors. The recovered potential was very good and the corresponding eigenvalues compared well with the noiseless exact ones. Statistical analysis on the errors propagated from the input noise was performed by computing the potential variance caused by the data errors based on the linearization assumption. Understanding the interplay between the data errors and the potential errors should aid in the treatment of true experimental data.

The illustrative example here with a diatomic potential also paves the way for the study of polyatomic, mainly triatomic, molecular potentials. This is particularly attractive due to the general availability of the highly accurate experimental spectral data. Our ultimate goal is to incorporate the newly developed numerical procedures for solving forward bound state polyatomic problems¹⁷ into the RIFSA method to determine their multidimensional potential surfaces.

ACKNOWLEDGMENTS

This work has been supported by grants from the Department of Energy, and the Donors of the Petroleum Research Fund, administered by the American Chemical Society. The authors would like to thank Dr. R. J. Le Roy for the program to solve the radial Schrödinger equation for bound levels.

¹ (a) T.-S. Ho and H. Rabitz, *J. Chem. Phys.* **89**, 5614 (1988); **90**, 1519 (1989); (b) **91**, 7590 (1989); (c) **94**, 2305 (1991).

² (a) R. Rydberg, *Z. Phys.* **73**, 376 (1931); (b) O. Klein, *ibid.* **76**, 226 (1932); (c) A. L. G. Rees, *Proc. Phys. Soc.* **59**, 998 (1947).

³ (a) S. M. Kirschner and J. K. G. Watson, *J. Mol. Spectrosc.* **51**, 321 (1974); (b) C. Schwartz and R. J. Le Roy, *J. Chem. Phys.* **81**, 3996 (1984).

⁴ (a) R. M. Roth, M. A. Ratner, and R. B. Gerber, *Phys. Rev. Lett.* **52**, 1288 (1984); (b) M. A. Ratner and R. B. Gerber, *J. Phys. Chem.* **90**, 20 (1986); (c) R. B. Gerber, *Comments At. Mol. Phys.* **17**, 65 (1985); (d) D. J. Nesbitt, M. S. Child, and D. C. Clary, *J. Chem. Phys.* **90**, 4855 (1989).

⁵ W. M. Kosman and J. Hinze, *J. Mol. Spectrosc.* **56**, 93 (1975).

⁶ C. R. Vidal, *Comments At. Mol. Phys.* **17**, 173 (1986), and references therein.

⁷ C. R. Vidal and H. Scheingraber, *J. Mol. Spectrosc.* **65**, 46 (1977).

⁸ I. P. Hamilton, J. C. Light, and K. B. Whaley, *J. Chem. Phys.* **85**, 5151 (1986).

⁹ (a) A. N. Tikhonov and V. Y. Arsenin, *Solutions of Ill-posed Problems* (Winston/Wiley, Washington D.C., 1977); (b) M. Bertero, C. De Mol, and E. R. Pike, *Inverse Problems* **4**, 573 (1988).

¹⁰ (a) M. Bertero, C. De Mol, and E. R. Pike, *Inverse Problems* **1**, 301 (1985); (b) O. N. Strand, *SIAM J. Numer. Anal.* **11**, 798 (1974).

¹¹ C. Schwartz and R. J. Le Roy, *J. Mol. Spectrosc.* **121**, 420 (1987); R. J. Le Roy (private communication).

¹² We used the computer code written by R. J. Le Roy for solving the

- radial Schrödinger equation for bound and quasibound levels; also see Ref. 11.
- ¹³P. M. Morse, *Phys. Rev.* **34**, 57 (1929).
- ¹⁴G. H. Golub and C. F. Van Loan, *Matrix Computations* (Johns Hopkins University, Baltimore, 1983).
- ¹⁵G. E. Backus and J. F. Gilbert, *Philos. Trans. R. Soc. London Ser. A* **266**, 123 (1970).
- ¹⁶D. S. Gilliam, J. R. Lund, and C. R. Vogel, *Inverse Problems* **6**, 725 (1990).
- ¹⁷Z. Bačić and J. C. Light, *Annu. Rev. Phys. Chem.* **40**, 469 (1989).